Journal of Power Sources 196 (2011) 9612–9617

Contents lists available at ScienceDirect

Journal of Power Sources

journal homepage: www.elsevier.com/locate/jpowsour

Characterization of Na-based phosphate as electrode materials for electrochemical cells

K. Zaghib[a,*], J. Trottier[a], P. Hovington[a], F. Brochu[a], A. Guerfi[a], A. Mauger[b], C.M. Julien[c]

[a] Institut de Recherche d'Hydro-Québec, 1800 Bd Lionel-Boulet, Varennes, Québec, Canada J3X 1S1
[b] Université Pierre et Marie Curie – Paris-6, IMPMC, Tour 23, 4 Place Jussieu, 75005 Paris, France
[c] Université Pierre et Marie Curie – Paris-6, PECSA, UMR 7195, Bat. F74, 4 Place Jussieu, 75005 Paris, France

ARTICLE INFO

Article history:
Received 14 May 2011
Received in revised form 17 June 2011
Accepted 18 June 2011
Available online 25 June 2011

Keywords:
Maricite
Olivine
Sodium insertion
Na cells

ABSTRACT

We report the electrochemical properties of submicron-sized particles of $NaFePO_4$. Two materials have been studied and characterized by XRD, SEM, EDX, EIS and Raman experiments: the maricite phase synthesized by hydrothermal method and the olivine phase obtained from delithiation of $LiFePO_4$. $NaFePO_4$ materials have an electrochemical activity in Na cell using $NaPF_6$–EC–DEC electrolyte, but only in the heterosite phase, and the capacity is reduced already in the second cycle. The two-phase system at intermediate compositions has also been analyzed.

1. Introduction

Because the low cost and abundance of sodium, there is a renewed interest in the development of Na-based electrodes, especially those that can be synthesized by hydrothermal method. In the past, several compounds have been investigated such as Na_xCoO_2 exhibiting different phases depending of its synthesis conditions [1]. Sodium insertion in vanadium oxides, i.e. the one-channel structure (β-$Na_xV_2O_5$) and two layered structures ($Na_{1+x}V_3O_8$ and α-V_2O_5), have been studied with regard to their use as cathode materials in solid-state sodium batteries. Both $Na_{1+x}V_3O_8$ and β-$Na_xV_2O_5$ battery cycle lives are very poor. The structure of α-V_2O_5 changes after the first discharge, but the new phase exhibits excellent capacity retention upon cycling [2]. Electrochemical insertion of sodium into phosphates $Na_3Fe_2(PO_4)_3$ has shown that Na^+ ions can be accommodated into this host [3]. More recently, a highly reversible capacity of ca. 120 mAh g^{-1} has been reported for $NaCrO_2$ in Na cell, with suitable capacity retention [4]. Liu et al. [5] have synthesized by hydrothermal route NaV_6O_{15} nanorods that performed stable Na-ion insertion–extraction. However, the poor reversibility and the low capacity of all these materials are far from the expected targeted performance for Na batteries.

Similarly to $LiFePO_4$ [6,7], $NaFePO_4$ might be a good candidate as electrode materials in electrochemical cells. Known for their excellent redox abilities and thermal stability, transition metal polyphosphates have been studied in great detail. To date, $NaFePO_4$ is not well-documented or characterized in Na cells, and some workers have stated that it is not viable as a cathode material. The reason evoked by Ellis et al. is that the closed maricite framework results in entrapment of Na^+ and no reversible redox behaviour [8]. However, such claims have never been verified by substantial experiments. Recham et al. [9] have shown the Na-cells with Na_2FePO_4F positive electrode display charge–discharge profiles in the 3-V region. Moreau et al. [10] have reported the structure and phase stability of Na intercalated $FePO_4$ olivine.

In this work, we have synthesized $NaFePO_4$ materials using the hydrothermal route. Various conditions have been considered, such as chemical nature of precursors, molar stoichiometry, and pH of the starting solution. The structural characterization of Na-based electrode materials includes X-ray diffraction (XRD), scanning electron (SEM), transmission electron microscopy (TEM), energy dispersive spectroscopy (EDX) and Raman scattering experiments. Electrochemical properties such as galvanostatic discharge–charge and electrochemical impedance spectroscopy, have also been evaluated as a function of the synthetic conditions.

2. Experimental

2.1. Synthesis

We used two different routes to prepare the $NaFePO_4$ phases. First, the hydrothermal route using iron sulphate, sodium hydrox-

* Corresponding author. Tel.: +1 450 652 8019; fax: +1 450 652 8424.
E-mail address: zaghib.karim@ireq.ca (K. Zaghib).

0378-7753/$ – see front matter © 2011 Elsevier B.V. All rights reserved.
doi:10.1016/j.jpowsour.2011.06.061

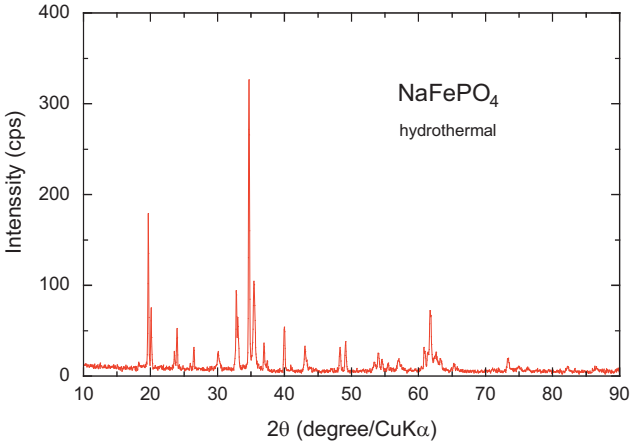

Fig. 1. XRD pattern of the $NaFePO_4$ maricite phase synthesized by hydrothermal method.

ide and H_3PO_4 as precursors. $FeSO_4$ + NaOH were mixed in aqueous solution for 6 h followed by incorporation of H_3PO_4 to adjust a solution at pH 8. Powders crystallized in the maricite phase were grown in autoclave at 165–200 °C for 7 h ($p \approx 200$ bars). Second, the electrochemical insertion of sodium into the $FePO_4$ heterosite was made after chemical delithiation of the triphylite $LiFePO_4$. The initial material, i.e. a carbon-coated $LiFePO_4$ sample, was prepared according to the "P2" industrial process of Süd-Chemieby hydrothermal process. Then, the delithiation was obtained by mixing $LiFePO_4$ powder with bromine dissolved in water and stirred at room temperature for 24 h. The powders were washed, filtered and dried at 200 °C. We also tried chemical delithiation by the $K_2S_2O_8$ method, but the delithiation of $LiFePO_4$ in that case failed to be complete. As a consequence, the lithium ions that had remained in the sample acted as impurities preventing the sodium to intercalate the matrix, leading to non-homogeneous Na content and very poor electrochemical performance. Only the results obtained with the delithiation by the bromine method are presented hereunder. To insert Na, $FePO_4$ was used as the positive electrode of the same Na cell as the one used to investigate the electrochemical properties.

2.2. Electrochemistry

The electrochemical properties of $NaFePO_4$ were tested at room temperature in cells with metallic sodium as anode electrode. Charge–discharge tests were performed on a coin type cell (CR2032). The composite positive electrode was prepared by thoroughly mixing the active material (90 wt.%) with carbon black (2 wt.%), acetylene black (2 wt.%), polyvinylidene fluoride (6 wt.%) in *N*-methyl-pyrrolidinone and spread onto aluminium foils, then dried for 24 h at 120 °C in vacuum. The active material was $NaFePO_4$ maricite powder, or $FePO_4$ obtained after chemical delithiation. The cells were then assembled in an argon-filled glove box using foils of Na metal as counter electrode and Celgard 2400 as separator. The electrolyte was 1.0 mol L^{-1} $NaPF_6$ in a mixture of ethylene carbonate (EC) and diethyl carbonate (DEC) (1:1, v/v). The cells were galvanostatically cycled between 1.7 V and 4.0 V vs. Na^0/Na^+ on a Mac-Pile battery tester at room temperature.

2.3. Apparatus

Structural analysis of the $NaFePO_4$ were characterized with X-ray diffraction (XRD) on a Philips X'Pert PRO MRD (PW3050) diffractometer equipped with a Cu anticathode (Cu Kα radiation $\lambda = 1.54056$ Å) at room temperature. XRD patterns were collected under Bragg–Brentano geometry at 2θ with step 0.025° in the range 10–80°. For morphological analysis, a scanning electron microscope (SEM) study of the samples was performed using a Hitachi (Japan) electron microscope. The Raman scattering (RS) spectra were recorded on a Horiba–Jobin–Yon system equipped with a confocal microscope (50× objective). The 632.8 nm line of a He–Ne laser was used as excitation light. Spectra were recorded with acquisition time 30 s, and the spectral resolution was 2 cm^{-1}. All post-mortem analyses were carried out in neutral atmosphere to prevent oxidation of the sodium.

3. Results and discussion

3.1. The maricite phase

Fig. 1 shows the X-ray diffraction pattern of $NaFePO_4$ synthesized by hydrothermal method. The powders are crystallized in the orthorhombic structure (*Pnma* space group of the primitive cell) of the maricite mineral (Fig. 2), in agreement with prior results [11,12]. Lattice parameters calculated by a least square fitting method are $a = 9.001(1)$ Å, $b = 6.874(2)$ Å, $c = 5.052(5)$ Å and $V = 312.6(3)$ $Å^3$. We note that the elementary cell volume is slightly larger than for $LiFePO_4$ olivine structure ($V = 291.2$ $Å^3$) as the ionic volume of Na^+ is almost twice that of Li^+.

Crystallographic data are available in the literature for $NaFePO_4$ maricite as well as for $NaFePO_4$ olivine [12–14]. In maricite-like $NaFePO_4$, the PO_4^{3-} anions occupy the 4*c* sites, while Na^+ and Fe^{2+} cations occupy 4*c* and 4*a* sites, respectively. O_1 is located in the 8*d* sites, O_2 and O_3 occupy the 4*c* sites. In the olivine $LiFePO_4$ structure

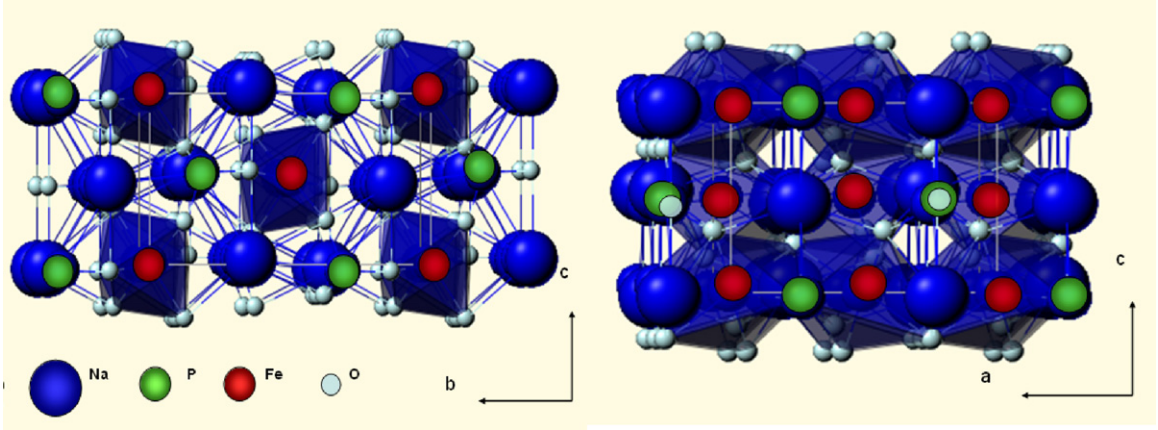

Fig. 2. Representation of the maricite structure (*Pnma* S.G.) along the orthorhombic a- and b-crystallographic axis.

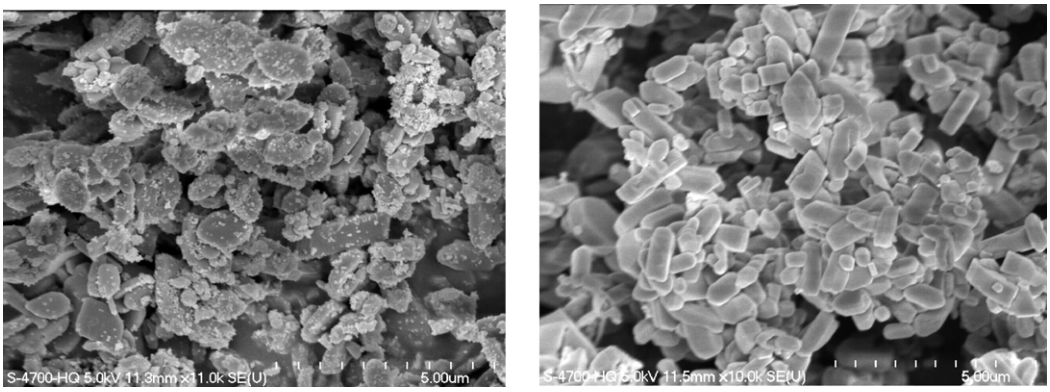

Fig. 3. SEM image of $NaFePO_4$ grown (a) before and (b) after optimization of the hydrothermal method.

(*Pnma* S.G.), the divalent iron ions are octahedrally coordinated and occupy 4*c* sites; while Li ions are situated on 4*a* octahedral sites [15].

The average mono-crystallite size was calculated from the XRD line width using the Scherrer's formula, $d = 0.9\lambda/\beta_{1/2}\cos\theta$, where λ is the X-ray wavelength, $\beta_{1/2}$ is the corrected width at half-height of the main diffraction peaks, and θ is the diffraction angle. The procedure to determine $\beta_{1/2}$ has been reported elsewhere [16]. The parameter d has been measured for different angles. No significant dependence on θ has been evidenced, and the result is $d = 160 \pm 8$ nm. The morphology of $NaFePO_4$ powders is depicted by the SEM images shown in Fig. 3. The prismatic shape of particles grown after subsequent calcination with average size 400 nm × 800 nm indicates that the particles are made of several crystallites.

The local structure of $NaFePO_4$ was investigated by optical spectroscopy. The Raman spectrum reported in Fig. 4 shows the well-developed stretching modes of $(PO_4)^{3-}$ structural units at ca. 900–1100 cm^{-1}. The FeO_6 stretching modes appear at ca. 661 and 703 cm^{-1}, while the bending modes of $(PO_4)^{3-}$ groups are observed below 600 cm^{-1}. The spectroscopic measurements display the well-organized local structure of the maricite phase [14]. No extrinsic peak is observed. The well-resolved asymmetric and symmetric stretching modes of the tetrahedral PO_4 groups give evidence of the good crystallinity and the purity of the $NaFePO_4$ maricite powder prepared by hydrothermal method. The factor group splitting, which is defined as the difference between the frequencies of highest and lowest bands in a given vibration multiplet [15], is 85 cm^{-1} for the ν_3 asymmetric mode of $NaFePO_4$, close to the value met in $LiFePO_4$ (82 cm^{-1}).

The electrochemical features of $NaFePO_4$ (maricite) cathode were investigated in coin-type cells cycled in the potential window 2–4 V vs. Na^0/Na^+. As a result, we found impossible to remove the sodium from the matrix. The cell behaved like a capacitor (not shown here). even at 60 °C operating temperature. This is due to the fact that there is no cation channel (see Fig. 2) contrary to the olivine phase. That is the reason why the efforts have been focused on the investigation of the olivine-based $NaFePO_4$ [10,17,18], which is the purpose of the next section.

3.2. The olivine phase

Insertion of sodium into the olivine host lattice was carried out from the complete chemical delithiation of $LiFePO_4$ as explained in the experimental section. The typical SEM image of the $FePO_4$ sample (Fig. 5) shows that the average particle size is in the range 500–600 nm. The $FePO_4$ sample was then used as the cathode material of the coin type cell (CR2032) described in Section 2, with Na metal as the anode.

The electrochemical properties measured at 60 °C at C/24 rate are reported in Fig. 6a and b. The discharge capacity is 147 mAh g^{-1} in the first cycle of the cell operating in the range 2–3 V (Fig. 6a) and up to 4 V (Fig. 6b). The plateau observed at circa 2.8 V is in agreement with prior results [10]. The difference with respect to the plateau recorded at 3.4 V vs. Li/Li^+ for $LiFePO_4$ is almost equal to the difference of standard oxidation–reduction potential between Na/Na^+ and Li/Li^+ [10], which gives evidence that the Na interca-

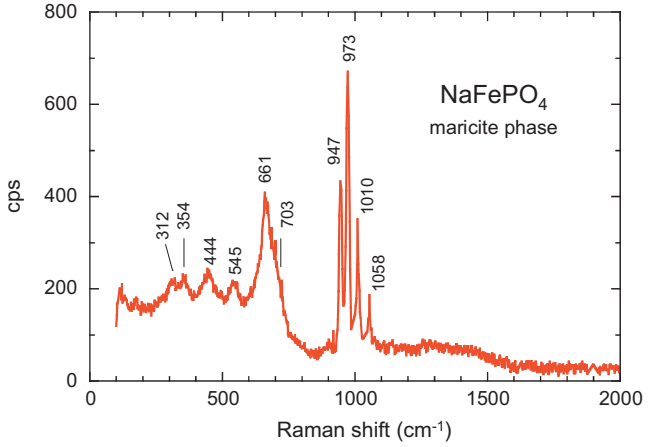

Fig. 4. Raman scattering spectrum of the $NaFePO_4$ maricite phase synthesized by hydrothermal route.

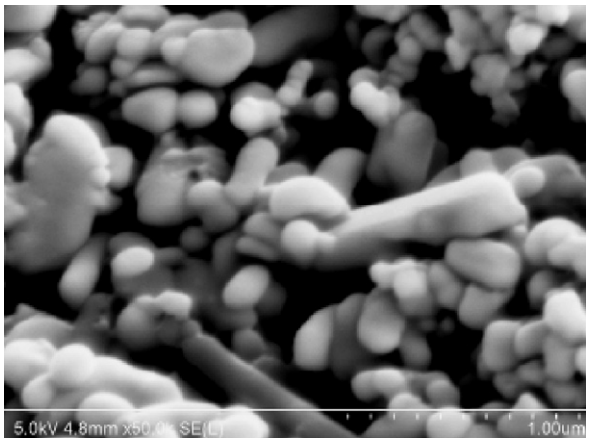

Fig. 5. SEM image of the heterosite $FePO_4$ sample obtained by the complete delithiation of $LiFePO_4$ powders using the bromine method.

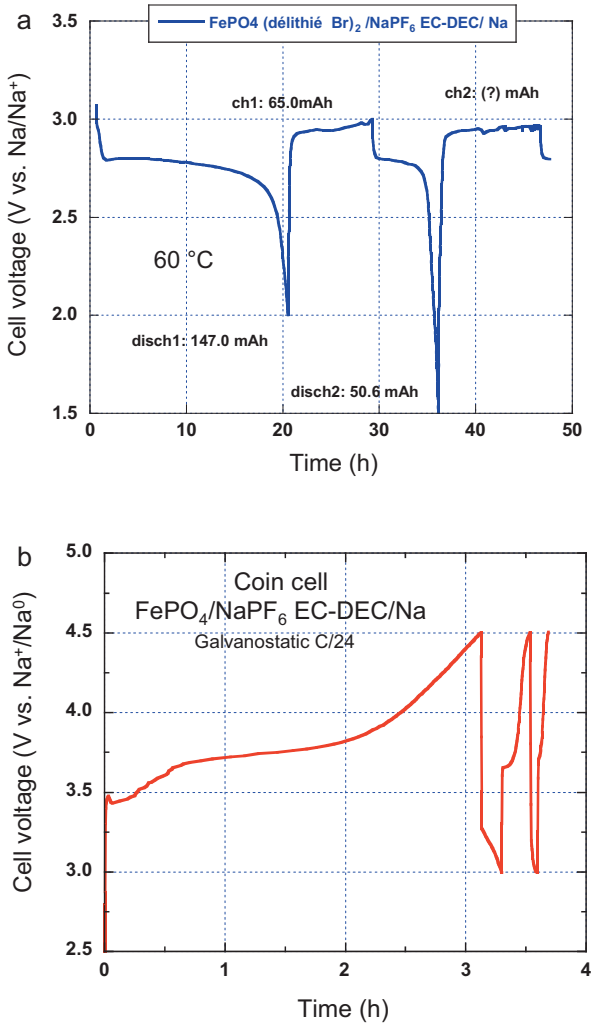

Fig. 6. Discharge–charge curves of a $Na/NaPF_6$ in EC–DEC/$FePO_4$ cell at C/24 rate in the potential window 3.0–1.5 V (a) and 3.0–4.5 V (b). The cathode material is the heterosite $FePO_4$ obtained by chemical delithiation of $LiFePO_4$ and carbon-coated using lactose method.

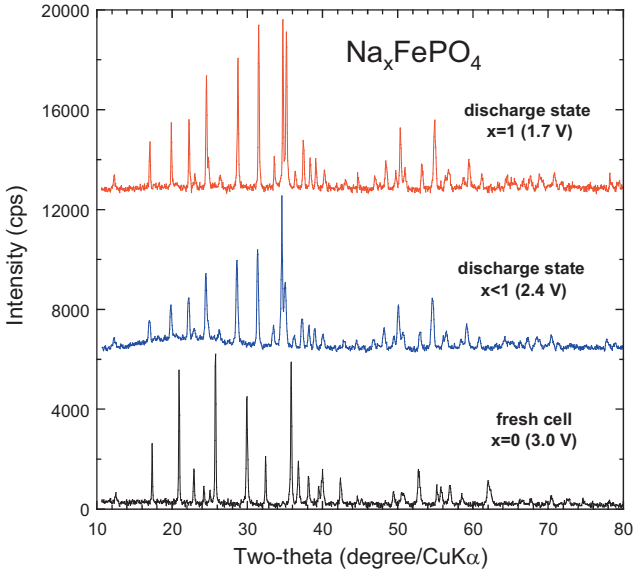

Fig. 7. XRD diagrams of Na_xFePO_4 after insertion of Na into the $FePO_4$ olivine host. Ex situ patterns were recorded for cells in the discharge state at 2.4 V and 1.7 V vs. Na^0/Na^+. The XRD pattern of the electrode (heterosite phase) in fresh cell is shown for comparison. Elemental analyses have shown that $x = 1$ at 1.7 V.

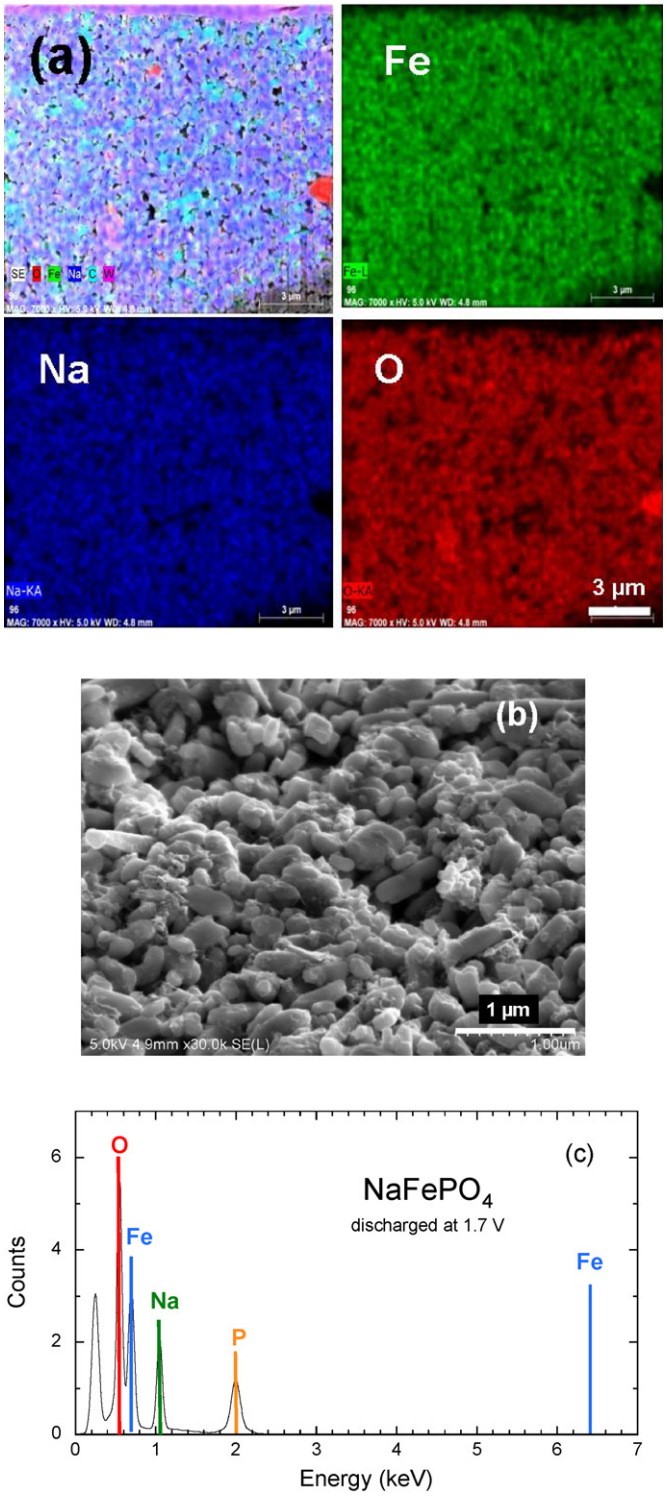

Fig. 8. (a) Elemental analysis EDX images of $NaFePO_4$ (discharged at 1.7 V), in which we note the homogeneous distribution of sodium in the analyzed area. (b) SEM image of the same electrode material. (c) Elemental analysis EDX spectrum.

lation site in $FePO_4$ is the same as that of Li in $LiFePO_4$. When the cell was charged up to 4 V, the following cycles show very poor reversibility despite the voltage profile similar to that reported by Moreau et al. [10]. When the upper voltage was limited to 3 V, the cyclability was better, i.e. 50.6 mAh was delivered at the 2nd cycle. Nevertheless, the cyclability did not exceed 4–5 cycles. Burba and Frech have reported the galvanostatic discharge of the $FePO_4$ structure in a Na-cell. The Na insertion was found along a flat plateau

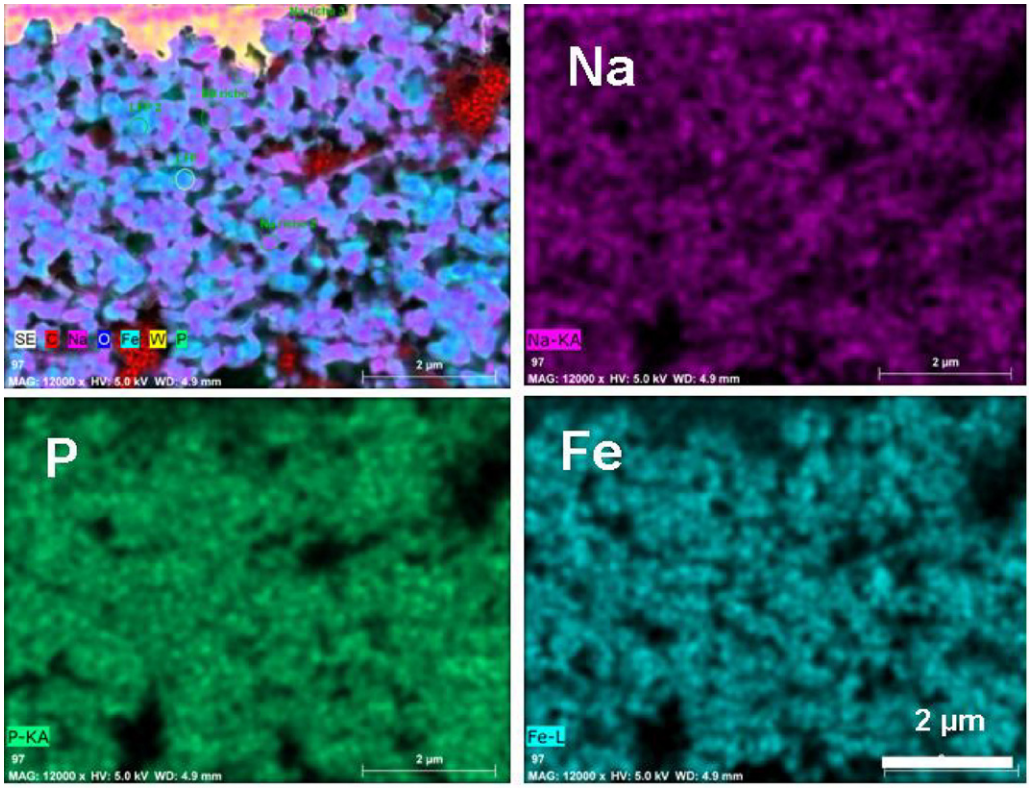

Fig. 9. Elemental analysis by EDX of Na_xFePO_4 (discharged at 2.4 V). Note the non homogeneous concentration of Na^+ ions in some regions.

of 2.87 V vs. Na^0/Na^+ with a first discharge capacity of 151 mAh g^{-1} that corresponds to the $Na_{0.85}FePO_4$ stoichiometry [15]. From the point of view of lattice dynamics, the spectroscopic features of $NaFePO_4$ electrochemically prepared show that this compound is structurally related to $LiFePO_4$, but the splitting of the intramolecular PO_4^{3-} vibrations suggests stronger interactions between ions in the elementary cell.

Fig. 7 shows the XRD diagrams of Na_xFePO_4 before and after insertion of Na into the $FePO_4$ olivine host. Ex situ patterns were recorded for cells discharged at 2.4 V and 1.7 V vs. Na^0/Na^+. The XRD pattern of the fresh electrode ($x = 0$) is also reported for comparison. Elemental analyses have shown that $x = 1$–1.7 V. Additional evidence that the olivine structure has been conserved is given by the XRD spectrum obtained after full discharge of the cell at 1.7 V (Fig. 7). This XRD spectrum of $NaFePO_4$ is in quantitative agreement with prior results reported in the literature and the heterosite structure has been conserved; only the lattice parameters have changed [19]. However, a close observation of the XRD pattern of the discharged electrode shows a double set of peaks. In particular the (3 1 1) Bragg line is split in a doublet at $2\theta = 34.7^\circ$ and 35.2°. This is attributable to the coexistence of the $Na_{0.7}FePO_4$ and the $NaFePO_4$ phases that have been identified in [10]. This is also consistent with the second plateau observed at 3.7 V in Fig. 6b.

We have completed the study of the insertion of Na in Na_xFePO_4 by energy-dispersive X-ray (EDX) elemental analysis. The results are reported in Fig. 8 for the sample charged at 1. 7 V (a) along with the SEM image (b) of this discharged electrode ($x = 1$). Fig. 9 shows similar experiments for the electrode material taken at 2.4 V ($x < 1$). Note that the SEM images clearly show that $NaFePO_4$ particles have a shape similar to the initial $FePO_4$ olivine without subsequent modification.

The analysis shown in Fig. 8 shows that the distribution of Na is homogeneous, and the ratio Na/P is equal to 1.0, which confirms that the full insertion of Na has been achieved at 1.7 V. On another hand, the analysis displayed in Fig. 9 at intermediate Na concentration shows quite an inhomogeneous distribution of Na, which is consistent with the two-phase nature of the intermediate state evidenced by the XRD analysis and the potential profile in Fig. 6a and b, which is characteristic of the two-phase system according to the Gibbs law. The black regions in the picture showing the Na distribution actually suggest that the Na concentration is close to zero in these area. Therefore, in first approximation, the miscibility gap extends to the whole diagram, and the notation Na_xFePO_4 can be considered as a short notation for a phase $FePO_4 + x$ $NaFePO_4$.

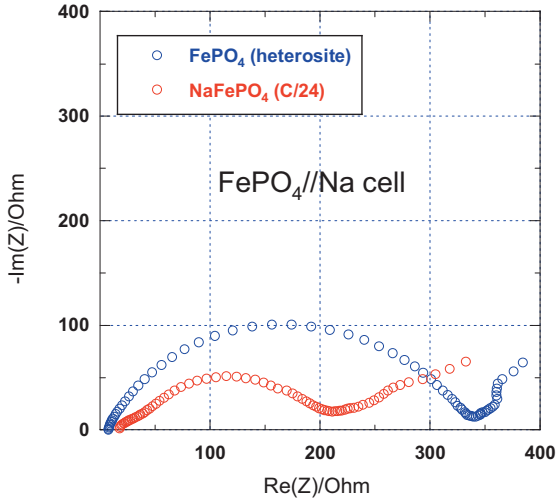

Fig. 10. EIS diagram of the cell after discharge $Na/NaPF_6$ in $EC–DEC/FePO_4$ cell. The cathode material is the heterosite $FePO_4$ obtained by chemical delithiation of $LiFePO_4$.

The electrochemical impedance spectroscopy (EIS) measurements of the cell after discharge at 1.7 V were carried out using perturbation voltage amplitude 10 mV in the frequency range from 100 kHz to 50 mHz. The results reported in Fig. 10 show the classical behaviour of a single semi-circle, followed at low frequency by a more linear part that is too small, however, to be analyzed in terms of a Warburg contribution. These results show that there is an ionic conductivity, but the resistance after full discharge is much smaller than that of the fresh cell, and indeed, the capacity of the second cycle is much smaller than in the first cycle, as shown in Fig. 6.

4. Conclusion

We have successfully synthesized the maricite phase of $NaFePO_4$ that is the most stable phase for this material. When optimization of the hydrothermal reaction was done, prismatic particles with average size 400 nm × 800 nm were obtained after subsequent calcination. Raman spectroscopy confirms the well-developed local environment of iron $Fe^{2+}O_6$ sublattice in the orthorhombic phase. Sodium iron phosphate does not show any significant electrochemical activity for the Na insertion in this maricite host. The capacity retention is reduced to few mAh g^{-1} for Na^+ ion insertion, due to the absence of channels in the maricite structure. On another hand, the discharge capacity of 147 mAh g^{-1} could be obtained for $NaFePO_4$ in the olivine phase, and full insertion of Na can be achieved at 1.7 V. The complete delithiation of $LiFePO_4$ to obtain the starting $FePO_4$ material before the insertion of Na is crucial to obtain such a result, because Li ions remaining in the matrix are defects that block the insertion of Na in the channels, since the insertion site of Na is the same as that of Li in the $FePO_4$ matrix. However, the capacity decreases very fast with the cycle number. The results also suggest that the sodium insertion/de-insertion operates in a two-phase process similar to that of Li [20,21].

References

[1] C. Fouassier, G. Matejka, J.M. Réau, P. Hagenmuller, J. Solid State Chem. (1973) 532.
[2] K. West, B. Zachau-Christiansen, T. Jacobsen, S. Skaarup, Solid State Ionics 28–30 (1988) 1128.
[3] Z. Znaidi, S. Launay, M. Quarton, Solid State Ionics 93 (1997) 273.
[4] S. Komaba, C. Takei, T. Nakayama, A. Ogata, N. Yabuuchi, Electrochem. Commun. 12 (2010) 355.
[5] H. Liu, H. Zhou, L. Chen, Z. Tang, W. Yang, J. Power Sources 196 (2011) 814.
[6] A.K. Padhi, K. Nanjundaswamy, J.B. Goodenough, J. Electrochem. Soc. 144 (1997) 1188.
[7] C.M. Julien, A. Mauger, A. Ait-Salah, M. Massot, F. Gendron, K. Zaghib, Ionics 13 (2007) 395.
[8] B.L. Ellis, W.R.M. Makahnouk, Y. Makimura, K. Toghill, L.F. Nazar, Nat. Mater. 6 (2007) 749.
[9] N. Recham, J.-N. Chotard, L. Dupont, K. Djellab, M. Armand, J. Electrochem. Soc. 156 (2009) A993.
[10] P. Moreau, D. Guyomard, J. Gaubicher, F. Boucher, Chem. Mater. 22 (2010) 4126.
[11] P.R. Tremaine, C. Xiao, J. Chem. Thermodyn. 31 (1999) 1307.
[12] J.N. Bridson, S.E. Quinlan, P.R. Tremaine, Chem. Mater. 10 (1998) 763.
[13] Y. Le Page, G. Donnay, Can. Mineral. 15 (1997) 518.
[14] M.T. Paque-Ledent, Rev. Chim. Miner. 10 (1973) 785.
[15] C.M. Burba, R. Frech, Spectrochim. Acta A65 (2006) 44.
[16] N. Amdouni, K. Zaghib, F. Gendron, C.M. Julien, Ionics 12 (2006) 117.
[17] N. Le Poul, E. Baudrin, M. Morcrette, S. Gwizdala, C. Masquelier, J.M. Tarascon, Solid State Ionics 159 (2003) 149.
[18] T. Shiratsuchi, S. Okada, J. Yamaki, T. Nishida, J. Power Sources 159 (2006) 268.
[19] G. Kobayashi, S.-I. Nishimura, M.-S. Park, R. Kanno, M. Yashima, T. Ida, A. Yamada, Adv. Funct. Mater. 19 (2009) 395.
[20] M.L. Trudeau, D. Laul, R. Veillette, A.M. Serventi, K. Zaghib, A. Mauger, C.M. Julien, J. Power Sources 196 (2011) 7383–7394.
[21] C.M. Julien, A. Mauger, K. Zaghib, J. Mater. Chem. 21 (2011) 9955–9968.